Global optimization of small bimetallic Pd–Co binary nanoalloy clusters: a genetic algorithm approach at the DFT level†

Mikail Aslan,[a] Jack B. A. Davis[b] and Roy L. Johnston*[b]

The global optimisation of small bimetallic PdCo binary nanoalloys are systematically investigated using the Birmingham Cluster Genetic Algorithm (BCGA). The effect of size and composition on the structures, stability, magnetic and electronic properties including the binding energies, second finite difference energies and mixing energies of Pd–Co binary nanoalloys are discussed. A detailed analysis of Pd–Co structural motifs and segregation effects is also presented. The maximal mixing energy corresponds to Pd atom compositions for which the number of mixed Pd–Co bonds is maximised. Global minimum clusters are distinguished from transition states by vibrational frequency analysis. HOMO–LUMO gap, electric dipole moment and vibrational frequency analyses are made to enable correlation with future experiments.

A. Introduction

The structural characterisation of clusters and nanoparticles is key in elucidating the size-dependent properties of nanoscale materials to facilitate many potential applications. Geometric structures of small nanoparticles (or subnanometre clusters) can be determined by coupling experimental measurements with theoretical calculations.[3] The generation of possible geometric isomers that can be used to explain experimental findings can be made by intuition[4–6] but this becomes impossible for larger systems and will also bias results. Another approach is to utilise an algorithm that explores configurational space to determine the global minimum (GM). Several computational methods that predict the globally stable structures of subnanometre clusters are available, such as statistical mechanical methods,[7,8] basin hopping[9] and genetic algorithms (GA).[10] The choice of technique depends on how the potential energy surface is described and how complex it is.[11,12] After the optimisation of the cluster structure using these methods, reoptimisation at the Density Functional Theory (DFT) level can be performed in order to correlate the predicted lowest energy structure with experimental results for free or supported clusters.[13–15]

Experimental findings associated with theoretical investigations have revealed that the bonding situation for clusters and small nanoparticles is generally different from the corresponding bulk material[16,17] and can also differ for two elements of the same group.[18] For these reasons, electronic structure calculations are needed to predict the correct growth characteristics of small clusters. Thus, due to growing interest in the design of novel functional nanomaterials, the DFT analysis of clusters of metals such as cobalt, platinum, palladium, silver, and gold has become a hot research field for chemists, physicists, and materials scientists.[19–33]

Clusters become more complex when two or more metals are alloyed in order to tune the characteristics of the particles not only by size but also by composition and chemical ordering, possibly resulting in special synergistic effects for these "nanoalloys".[34] In recent years, bimetallic nanoparticles have been studied using many body empirical potentials, with the GM predicted using a GA, often yielding consistent results with experiments.[35] However, an examination of the bonding in smaller (subnanometre) bimetallic clusters can only be achieved using electronic structure methods. For this reason, we have recently developed a program for the direct global optimisation of cluster geometries at the DFT level – the so-called GA-DFT approach.[3,36] Another motivation is that nanoalloy particles often have superior chemical and physical properties compared to single element nanoparticles.[37] Thus, nanoalloys are of great interest in the chemical industry: for example, one metal may adjust the catalytic properties of the other due to structural and/or electronic effects. In many nanoalloys, the lowest energy configurations have a core of one metal surrounded by a shell of the other metal, so that smaller volumes of a catalytically active element (thereby reducing the cost) might be sufficient to achieve similar effects as those of

[a] *Department of Metallurgical and Materials Engineering, Gaziantep University, Gaziantep, Turkey*

[b] *School of Chemistry, University of Birmingham, Birmingham, UK.*
   E-mail: r.l.johnston@bham.ac.uk

single element catalysts.[38] Furthermore, in Fisher–Tropsch catalysis,[39–41] PdCo nanoparticles have been shown to display higher selectivity than pure Co particles. Synthesis of hydrocarbon fuels by reacting carbon monoxide and hydrogen is appealing to many researchers in this area due to recent huge fluctuations in the prices of hydrocarbons.[38]

In this paper, we have used the Birmingham Cluster Genetic Algorithm (BCGA) with an interface to the PWscf DFT code within the Quantum Espresso (QE) package. This provides an unbiased search starting from entirely random coordinates for the search of GM of PdCo nanoalloys. Here we conduct the first GM search for 4–7 atom PdCo bimetallic nanoalloys, over the entire composition range, using the GA-DFT approach.

B. Methods

In the present study, the putative GM isomers are generated by the Birmingham Cluster Genetic Algorithm (BCGA)[10] within the framework of Density Functional Theory, using an interface to the PWscf code of Quantum Espresso (QE) software.[42] The BCGA is used for the structural characterisation of nanoparticles and nanoalloys. The interface with QE enables the energy landscape of a system to be searched for the GM at the DFT level.

In the first step of the GA, a set of individuals is generated randomly to form an initial population of 10 members. Real valued Cartesian coordinates are chosen and each structure is relaxed by optimising the potential energy as a function of its coordinates. The BCGA is a "Lamarckian" type GA, which combines a GA step with a subsequent local minimisation of the energy. Each structure is assigned a fitness value such that the lowest energy structures correspond to highest fitness. In the GA-DFT approach, the energy of each member of the population is obtained from a PWscf DFT calculation. The crossover process (to generate a predetermined number of offspring) uses the roulette wheel selection criterion and the Deaven–Ho cut and splice method.[43] Mutation is accomplished using a number of schemes in the BCGA, such as atom displacement, cluster twisting, cluster replacement (used here), and atom permutation and is performed to improve population diversity. The process of selection, crossover, and mutation is reiterated for a predetermined maximum number of generations (here 200). However, if after a certain number of generations the lowest energy member of the population does not change, then the population is considered to have converged and the GA terminates.

Plane-wave PWscf calculations are conducted by applying ultrasoft type pseudopotentials[44] for all metallic species, including scalar relativistic effects.[45] We have adopted the Perdew–Burke–Ernzerhof (PBE) GGA exchange–correlation functional[46] that has been widely used in the treatment of small, mixed clusters. For the primary screening of the structures with BCGA, the default density cutoff convergence criterion is applied with energy cutoff of 50 Ry. The Methfessel–Paxton smearing scheme[47] with a value of 0.01 Ry is applied to aid metallic convergence.

Spin-polarised reminimisations of BCGA-DFT global minima were carried out using the orbital-based DFT package NWChem.[48]

PBE exchange–correlation functionals,[46] LANL2DZ basis sets and relativistic effective core pseudopotentials (ECPs)[49,50] were used for Pd and Co, where only the outer-most electrons are treated explicitly in the calculations. Default convergence criteria have been applied during calculations: 1×10^{-6} Hartree for energy and 5×10^{-4} Hartree a_0^{-1} for the energy gradient. Geometry optimisations were performed without any symmetry constraints for a range of electron spin multiplicities.

DFT binding energies (E_b) are calculated from

$$E_b = \frac{nE_{Pd} + mE_{Co} - E_{Pd_nCo_m}}{n + m} \quad (1)$$

where, n is the number of Pd atoms and m is the number of Co atoms.

To further illustrate the stability of the nanoalloys and their size dependent behaviour, we have considered the second finite difference in energy, which is a sensitive quantity that is frequently used as a measure of the relative stability of a particular cluster with respect to neighbouring sizes or compositions and is often compared directly with the relative abundances determined in mass spectroscopy experiments. For a fixed size cluster, the second finite different energy ($D_{n,m}$) of the isomer Pd_nCo_m is calculated as

$$D_{n,m} = E_{n+1,m-1} + E_{n-1,m+1} - 2E_{n,m} \quad (2)$$

where $E_{n,m}$ is the total energy of the Pd_nCo_m nanoalloy.

The mixing energies (E_m) are listed in Table 1 to provide a measure of the stability of the bimetallic clusters with respect to the monometallic ones or the energy associated with alloying. E_m is defined here as the (positive) quantity

$$E_m = -\left[E(Pd_nCo_m) - \frac{n}{n+m}E(Pd_{n+m}) - \frac{m}{n+m}E(Co_{n+m})\right] \quad (3)$$

Table 1 Physicochemical properties of PdCo nanoalloys[a]

Clusters	SM	SYM	E_b	E_m	Clusters	SM	SYM	E_b	E_m
Co$_3$	7	C_{2v}	1.45	—	Co$_6$	14	O_h	2.41 / 2.47[c]	—
PdCo$_2$	4	C_{2v}	1.62	0.60	PdCo$_5$	13	C_{4v}	2.38	0.16
Pd$_2$Co	3	C_{2v}	1.70	0.93	Pd$_2$Co$_4$	10	C_{2v}	2.35	0.32
Pd$_3$	2	D_{3h}	1.37 / 1.24[b]	—	Pd$_3$Co$_3$	7	C_1	2.30	0.38
Co$_4$	10	C_{2v}	1.79	—	Pd$_4$Co$_2$	6	C_{2v}	2.27	0.55
PdCo$_3$	7	C_s	1.86	0.29	Pd$_5$Co	3	C_{4v}	2.21	0.51
Pd$_2$Co$_2$	4	C_{2v}	1.93	0.57	Pd$_6$	2	D_{4h}	2.06 / 1.88[b]	—
Pd$_3$Co	3	C_{3v}	1.97	0.73	Co$_7$	15	C_1	2.51 / 2.45[c]	0.00
Pd$_4$	2	D_{2d}	1.78 / 1.63[b]	—	Pd$_1$Co$_6$	14	C_3	2.54	0.64
Co$_5$	11	C_s	2.10 / 2.29[c]	—	Pd$_2$Co$_5$	13	C_s	2.52	0.90
PdCo$_4$	8	C_{3v}	2.14	0.36	Pd$_3$Co$_4$	10	C_{2v}	2.50	1.13
Pd$_2$Co$_3$	7	C_{2v}	2.17	0.70	Pd$_4$Co$_3$	7	C_1	2.42	0.98
Pd$_3$Co$_2$	4	C_{2v}	2.15	0.82	Pd$_5$Co$_2$	6	C_s	2.36	1.00
Pd$_4$Co	3	C_{2v}	2.10	0.76	Pd$_6$Co$_1$	3	C_5	2.25	0.68
Pd$_5$	2	C_{4v}	1.91 / 1.74[b]	—	Pd$_7$	2	D_5	2.10 / 1.90[b]	0.00

[a] SM, spin moment in μ_B; SYM, point group symmetry; E_b, binding energy in eV per atom; E_m, mixing energy in eV. [b] Ref. 1. [c] Ref. 2.

C. Results and discussion

To check the validity of the computational method for the study of the bimetallic PdCo nanoalloys, the binding energies (BEs) of Pd and Co dimers were calculated as 0.76 and 1.03 eV per atom, respectively. The obtained results are in agreement with experimental[51–55] and theoretical results.[22,56–59] The BE of the PdCo dimer (1.21 eV) does not lie between those of Pd_2 and Co_2. However, Pd_nCo_m binary nanoalloys properties are expected to lie in between those of pure palladium and cobalt clusters (Fig. 1–4).

The ground state structure of the Co trimer is still controversial. In our calculation, the GM structure of Co_3 has been identified as a C_{2v} isosceles triangle, as previously reported.[57,60,61] Experimentally, it was reported[62] that the electron spin resonance spectrum of the cobalt trimer in an Ar/Kr matrix shows a
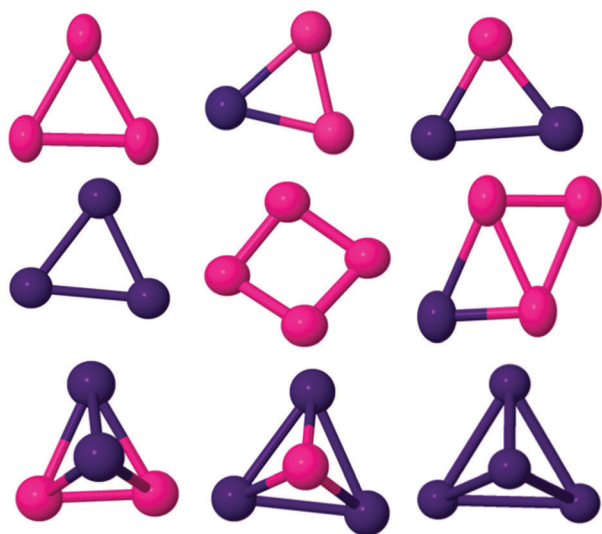

Fig. 1   Global minima for three and four atom PdCo nanoalloys. Pd and Co are shown in purple and pink, respectively.
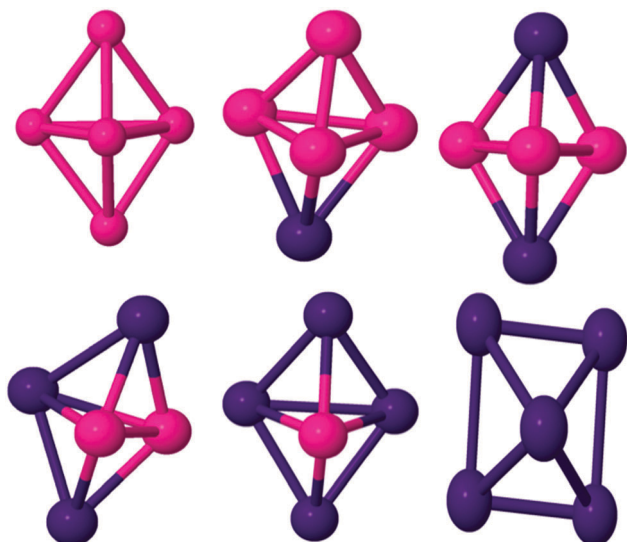

Fig. 2   Global minima for five atom PdCo nanoalloys.
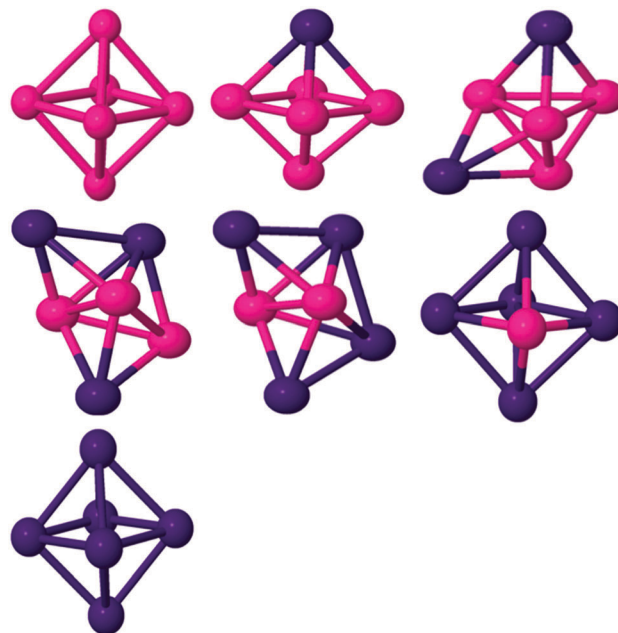

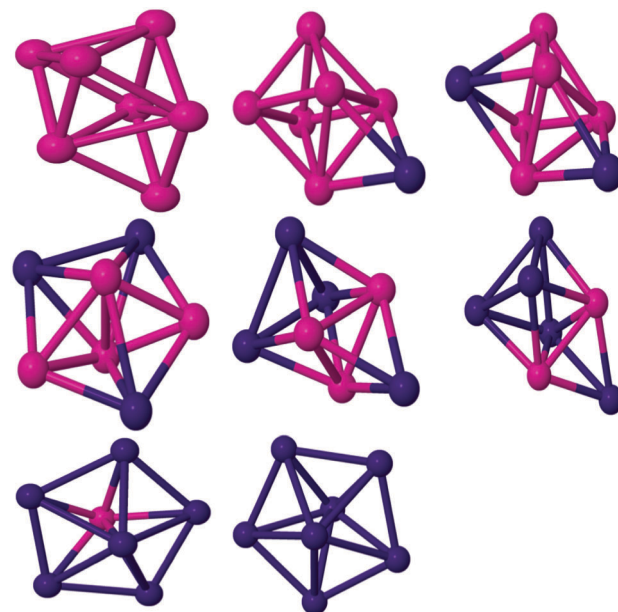Fig. 3   Global minima for six atom PdCo nanoalloys.

Fig. 4   Global minima for seven atom PdCo nanoalloys.

triangular structure with a spin moment of 5 or 7 μ_B. However, Co_3 was found to adopt a linear geometry in ref. 59 and 63. Datta et al.[61] found the BE and spin moment as 1.78 eV per atom and 5 μ_B respectively while we found corresponding values of 1.45 eV per atom and 7 μ_B respectively (see Table 1). By introducing up to two Pd dopant atoms into the cluster, the overall structural motif is not changed significantly (see Fig. 1). For the $PdCo_2$ cluster, an isosceles triangle with total magnetic moment 5 μ_B is found to be the GM with BE 1.62 eV per atom. The BE value is consistent with the result in ref. 38. When doped with two Pd atoms, the isosceles triangle remains the

GM while the pure Pd trimer has a D_{3h} equilateral triangle structure, though the calculated BE of this structure (1.37 eV per atom) is inconsistent with DFT results reported by other researchers.[64,65]

The most stable isomer of Co_4 is a non-planar butterfly-like structure with C_{2v} symmetry (as the two diagonals are unequal in length). It has a BE of 1.79 eV per atom and a spin moment of 10 μ_B, as reported by Sebetci,[59] Fan et al.,[2] and Ma et al.[66] but in contradiction to the findings of Datta et al.[67] Experimentally, Jalink et al.[68] identified Co_4 as having a planar rhombus structure based on a gas phase vibrational spectroscopy. Replacing one of the Co atoms by Pd, results in a non-planar butterfly as the lowest energy morphology (see Fig. 1) and the symmetry is reduced to C_s, which removes orbital degeneracy, increases the d electron bandwidth and reduces the local magnetic moment of Co. As Pd doping increases, the BE of Pd_2Co_2 increases to 1.93 eV per atom in the quintet magnetic state and the structure changes to a C_{2v} tetrahedron, where all faces are isosceles triangles. The structure of Pd_3Co is a C_{3v} tetrahedron. A triplet spin multiplicity with D_{2d} symmetry is found to be the GM structure of Pd_4, which has a D_{2d} distorted-tetrahedral structure. This agrees with the results of Zanti et al.[69] and Begum et al.[70]

For the Co pentamer, a distorted trigonal bipyramidal (TBP) structure has been found as the GM energy structure with a spin magnetic moment of 11 μ_B. There is no consensus on the structure of Co_5 in the literature. Pereiro et al.,[60] Datta et al.[61] and Castro et al.[58] have identified the ground state structure as the TBP configuration while a C_{4v} pyramidal structure has been proposed by Fan et al.[2] and Ma et al.[66] The Pd_2Co_3, Pd_3Co_2 and Pd_4Co clusters (see Fig. 2) all have C_{2v} TBP geometries, with spin moments of 7, 4 and 3 μ_B, respectively, while the $PdCo_4$ cluster has a C_{3v} TBP structure and a spin moment of 8 μ_B. In Pd_4Co and Pd_3Co_2, Co atoms preferably occupy the higher connectivity equatorial positions in the TBP, which maximise the number of Co–Co and Co–Pd bonds (both of which are stronger than Pd–Pd bonds). The preferential doping of Pd atoms into the lower-connected apical sites in $PdCo_4$ and Pd_2Co_3 is consistent with this. In the case of the pure Pd pentamer, the lowest energy morphology changes to square a pyramid with C_{4v} symmetry and a triplet magnetic state. This structure agrees with the work of Cantera and coworkers,[38] and Zanti and coworkers[69] while Jerzy and coworkers[71] identified the GM as a TBP.

For pure Co_6 the GM structure is a regular octahedron with O_h symmetry and a magnetic moment of 14 μ_B, which is entirely consistent with previous results.[61,66,72] On replacing one Co by Pd (see Fig. 3), the overall octahedral structure is retained. The GM structure has C_{4v} symmetry and a total magnetic moment of 13 μ_B. When Pd atom doping continues, a capped TBP (or bicapped tetrahedron) is found to be GM for Pd_2Co_4 (C_{2v}), Pd_3Co_3 (C_1) and Pd_4Co_2 (C_{2v}). As for the pentamers, the Co atoms preferentially occupy the higher coordinate sites and the Pd atoms occupy the low coordinate sites, leading to more Co–Co (and Co–Pd) and fewer Pd–Pd bonds, again correlating with bond strengths and bulk cohesive energies.[73] The overall effect is for core segregation of Co and surface segregation of Pd, with this core–shell type of segregation (which is related to the lower surface energy of Pd compared to Co, since the element having smaller surface energy and cohesive energy favours occupying the surface to minimise the total energy[74]) also predicted for larger PdCo clusters.[75] Janssens et al.[76] found that with fewer than 50 atoms, for Ag_nCo_m with $n \gg m$ the cobalt dopants occupy highly coordinated sites and are strongly bound, for clusters with $m \gg n$ the silver atoms are poorly coordinated surface atoms and are loosely bound. The GM structure of Pd_5Co is an octahedron (C_{4v} symmetry) in the quartet magnetic state. The BE of Pd_5Co has been calculated as 2.21 eV per atom. It should be noted that the dominant growth patterns for the studied bimetallic nanoalloys generally keep similar frameworks to those of the pure Co clusters. Pd_6 has a D_{4h} tetragonally distorted octahedral geometry. This is consistent with previous DFT studies.[65,77,78]

The most stable isomer of Co_7 is a capped octahedron-like structure. It has a BE of 2.51 eV per atom while Datta et al.[67] calculated the BE as 2.97 eV per atom. The structure has a spin moment of 15, which is consistent with the experimental result (2.36 ± 0.25 μ_B per atom[79]). For $PdCo_6$, the overall capped octahedron-like structure is retained (see Fig. 4). The GM structure has C_3 symmetry and a spin moment of 14 μ_B. A low symmetry C_s isomer, with a spin moment of 13 μ_B, is found to be the GM for Pd_2Co_5. On further Pd doping, the structural motif changes to a pentagonal pyramid for Pd_3Co_4. Pd_4Co_3 has C_1 symmetry and a spin moment of 7 μ_B. The BE of Pd_4Co_3 has been calculated as 2.42 eV. For Pd_5Co_2, this structural motif is retained. The spin moment of Pd_5Co_2 is calculated as 6 μ_B and it has C_s symmetry. On further Pd doping, the structural motif changes to the pentagonal bipyramid. The pentagonal bipyramid GM structure for Pd_7 is consistent with the findings of Kalita and Deka.[80] The BE of this structure in the doublet state is calculated as 2.10 eV per atom, which is consistent with the result of ref. 38.

The magnetic spin moments of the GM structures of PdCo clusters within the studied size range are shown in Fig. 5. The magnetic moments of bimetallic PdCo clusters exhibit a zigzag pattern upon successive addition of Pd atoms. It should be noted that all pure Pd clusters in this study have triplet magnetic ground states, which is consistent with the results of ref. 69. As the Pd atom has a closed shell electronic configuration ($4d^{10}$), to make a
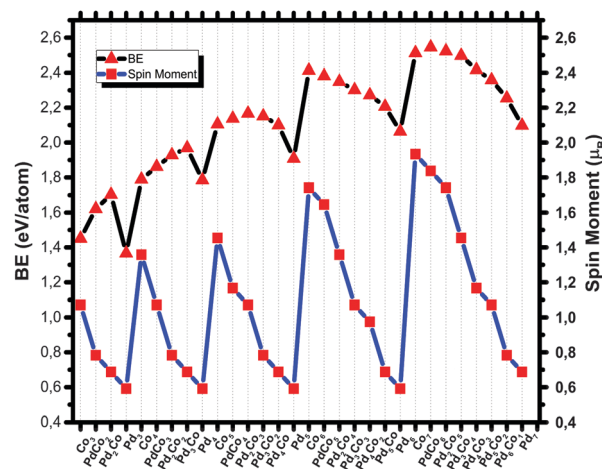

Fig. 5 Binding energies and spin moments of PdCo nanoalloys.

stable a metal–metal bond, some 4d electronic density needs to be promoted into the lowest unoccupied orbitals, in this case 5s. Occupying this orbital leads to a triplet state. As expected, Pd atoms have a quenching effect on the magnetism of bimetallic PdCo nanoalloys, so successive Pd doping of a Co cluster leads to a decrease of the spin moment of the ground state structure. We could not find any clear size dependence, but for CoMn clusters, based on Stern–Gerlach (SG) experiments, Yin et al.[81] have concluded that the magnetic enhancement of Co_nMn_m ($n \leq 60$, $m \leq n/3$) is independent of the cluster size and composition. However, the study conducted by Zanti and coworkers showed that clusters enriched in palladium atoms have spin multiplicities that increase with the cluster size while clusters enriched in gold atoms maintain the lowest possible spin multiplicity for the structure.[69]

Nanoparticle stability can be analyzed in various ways, the most common being the computation of the energy released during the growth of metal nanoparticles starting from isolated atoms, corresponding to the BE. The dependence of the BE on the composition of PdCo nanoalloys within the studied range is shown in Fig. 5. As expected, increasing nuclearity makes the BE larger. This is because during the growth process the number of nearest neighbors increases, leading to a larger number of inter-actions per atom but the proportional gain gets smaller as the cluster gets larger, eventually approaching the bulk cohesive energy asymptotically. For bimetallic PdCo clusters, the BE is expected to lie between those of pure Pd and Co clusters. However, up to size 5, the BEs are (as seen in Table 1) larger than both the pure Pd and Co clusters, while for size 6 and 7, the BE values usually lie between those of the pure Pd and Co nanoparticles, as expected. Bakken and Swang[82] have found that for small cobalt clusters, substituting rhenium stabilizes the clusters.

For the pentamer PdCo nanoalloys, Pd_4Co has a much higher $D_{n,m}$ energy than Pd_3Co_2. This shows that it is more stable than the latter species but the result is not consistent with the mixing energy result. For the hexamer structures, the dip is seen at Pd_3Co_3 in Fig. 6. This species is expected to be less abundant in mass spectra than the other corresponding clusters.

The mixing energy E_m can be used to evaluate the effect of mixing in a system. The evolution of the mixing energy with

Fig. 6 Second finite difference energies (D) and mixing energies (E_m) of 5–7-atom PdCo nanoalloys.

Table 2 Further physicochemical properties of PdCo nanoalloys[a]

Clusters	HLG	DM	FRQ	Clusters	HLG	DM	FRQ
Co_3	0.68	0.40	96, 231, 319	Co_6	0.32	0.00	120, 269, 344
$PdCo_2$	0.71	1.16	170, 170, 296	$PdCo_5$	0.29	0.52	81, 261, 318
Pd_2Co	0.76	0.75	148, 148, 286	Pd_2Co_4	0.50	0.25	78, 154, 301
Pd_3	0.01	0.13	159, 166, 237	Pd_3Co_3	0.37	0.72	66, 151, 287
Co_4	0.61	0.05	66, 233, 267	Pd_4Co_2	0.32	0.05	54, 257, 290
$PdCo_3$	0.59	1.32	46, 111, 290	Pd_5Co	0.54	0.74	83, 256, 256
Pd_2Co_2	0.51	1.35	111, 176, 289	Pd_6	0.08	0.00	99, 184, 220
Pd_3Co	0.48	0.84	95, 156, 285	Co_7	0.18	0.31	66, 253, 304
Pd_4	0.01	0.00	111, 184, 239	Pd_1Co_6	0.37	0.85	60, 254, 295
Co_5	0.52	0.53	74, 191, 327	Pd_2Co_5	0.33	0.64	85, 248, 299
$PdCo_4$	0.43	0.87	115, 192, 328	Pd_3Co_4	0.58	0.61	64, 151, 278
Pd_2Co_3	0.59	0.15	82, 256, 303	Pd_4Co_3	0.33	0.34	75, 257, 282
Pd_3Co_2	0.81	0.89	83, 173, 288	Pd_5Co_2	0.21	0.75	60, 122, 272
Pd_4Co	0.55	0.67	50, 238, 261	Pd_6Co_1	0.33	0.39	29, 226, 234
Pd_5	0.20	0.31	53, 195, 221	Pd_7	0.14	0.00	56, 167, 207

[a] HLG, HOMO–LUMO gap in eV; DM; electric dipole moment in Debyes; FRQ, lowest, weighted, highest vibrational frequencies, respectively, in cm^{-1}.

composition is shown for $n + m = 5$, 6 and 7 in Fig. 6. The more positive values of E_m show a stronger mixing tendency. The maximum value is seen for Pd_2Co in Table 1. This is consistent with the BE result. Comparing the different nuclearities, it should be noted that the mixing energy of bimetallic Pd_nCo_m nano-particles is independent of the cluster size. However, up to 6 atoms, the values of mixing energy of the studied nanoalloys are proportional to the proportion of Pd atoms in the cluster, with the exception of Pd_4Co and Pd_5Co.

A large HOMO–LUMO gap (HLG) is generally considered as a significant requirement for chemical stability since HLG indicates the ability of electrons to hop from HOMO to LUMO and indicates the tendency of a molecule to be involved in chemical reactions to some degree. Pd_3Co_2 (0.81 eV) has the highest HLG among the species studied in this work. Thus, one can expect high chemical stability for this cluster. It can be noted that pure Pd clusters generally have higher chemical activity than pure cobalt clusters. Furthermore, among the studied species, Pd-rich clusters are expected to have high chemical activity due to their low HLG values (see Table 2).

Electric dipole moment calculations have been performed to enable predictions to be made for future electron beam deflec-tion experiments, which is one of few experimental methods for the investigation of small neutral clusters. The dipole moments (see Table 2) are small due to the low charge distribution within the cluster with the exception of $PdCo_2$, $PdCo_3$ and Pd_2Co_2, which have clearly distinguishable dipole moments. These clusters should be easily discriminated by experiment.

The vibrational frequencies (see Table 2) lie between 29 and 344 cm^{-1} and show no clear dependence on cluster size and composition. All vibrational frequencies, projected infrared inten-sities, Mulliken charge analysis, electric field gradients, dipole, quadrupole and octupole moments are listed as ESI.†

D. Conclusions

We have performed a computational study of PdCo nanoalloys ranging from 3 to 7 atoms. The structural, electronic and
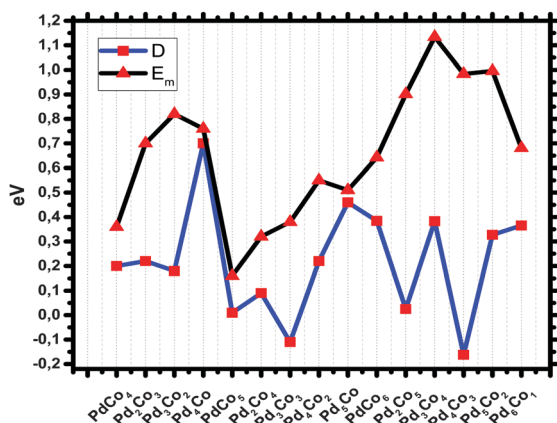
magnetic properties of bimetallic PdCo nanoalloys have been studied within the framework of the GA-DFT approach that performs an unbiased global optimisation search for the lowest energy isomer, for each size and composition, at the DFT level.

The calculations reveal that Pd atoms segregate to the peripheral positions of the clusters to enable maximisation of the stronger Co–Co and Co–Pd bonds and also the lower surface energy of Pd. Up to size 5, the doped nanoalloys possess higher binding energies indicating that the bimetallic species possess enhanced chemical stability than their pure counterparts. Pd atoms have a quenching effect on the magnetism of bimetallic PdCo nanoalloys, so successive Pd doping of a Co cluster leads to a decrease of the spin moment of the ground state structure. For the size dependence of magnetic moment we could not find any clear relation. It can be noted that pure Pd clusters generally have higher chemical activity than those pure cobalt clusters. Furthermore, among the studied species, Pd-rich clusters are expected to have high chemical activity due to their low HLG values. The dipole moments are small due to the low charge distribution within the cluster, with the exception of $PdCo_2$, $PdCo_3$ and Pd_2Co_2, which have clearly distinguishable dipole moments.

In the future, the study we have carried out will be extended to larger bimetallic PdCo nanoalloys, where the dependence of chemical ordering and structure on the composition will be analyzed by using the Pool-BCGA code,[83,84] which is a new parallel implementation of the code, which reduces computational costs significantly for larger clusters.

Acknowledgements

References

1 P. Nava, *Density Functional Theory Calculations on Palladium Clusters and on an AgInS Semiconductor Compound*, Cuvillier Verlag, 2005.

2 H.-J. Fan, C.-W. Liu and M.-S. Liao, *Chem. Phys. Lett.*, 1997, **273**, 353–359.

3 S. Heiles, A. J. Logsdail, R. Schafer and R. L. Johnston, *Nanoscale*, 2012, **4**, 1109–1115.

4 V. Bonačić-Koutecký, J. Burda, R. Mitrić, M. Ge, G. Zampella and P. Fantucci, *J. Chem. Phys.*, 2002, **117**, 3120.

5 H. M. Lee, M. Ge, B. R. Sahu, P. Tarakeshwar and K. S. Kim, *J. Phys. Chem. B*, 2003, **107**, 9994–10005.

6 G. F. Zhao and Z. Zeng, *J. Chem. Phys.*, 2006, **125**, 014303.

7 J. M. Montejano-Carrizales and J. L. Morán-López, *Surf. Sci.*, 1990, **239**, 169–177.

8 M. Polak and L. Rubinovich, *Surf. Sci.*, 2005, **584**, 41–48.

9 D. J. Wales and J. P. K. Doye, *J. Phys. Chem. A*, 1997, **101**, 5111–5116.

10 R. L. Johnston, *Dalton Trans.*, 2003, 4193–4207.

11 A. Sutton and J. Chen, *Philos. Mag. Lett.*, 1990, **61**, 139–146.

12 J. N. Murrell and R. E. Mottram, *Mol. Phys.*, 1990, **69**, 571–585.

13 B. C. Curley, R. L. Johnston, N. P. Young, Z. Li, M. Di Vece, R. E. Palmer and A. L. Bleloch, *J. Phys. Chem. C*, 2007, **111**, 17846–17851.

14 R. Ferrando, A. Fortunelli and R. L. Johnston, *Phys. Chem. Chem. Phys.*, 2008, **10**, 640–649.

15 O. Kostko, B. Huber, M. Moseler and B. von Issendorff, *Phys. Rev. Lett.*, 2007, **98**, 043401.

16 F. Chen and R. L. Johnston, *Acta Mater.*, 2008, **56**, 2374–2380.

17 F. Y. Chen and R. L. Johnston, *Appl. Phys. Lett.*, 2007, **90**, 3123.

18 J. Jellinek, *Faraday Discuss.*, 2008, **138**, 11–35.

19 L. B. Vilhelmsen and B. Hammer, *J. Chem. Phys.*, 2014, **141**, 044711.

20 A. Sebetci, *Comput. Mater. Sci.*, 2013, **78**, 9–11.

21 A. Sebetci, *Comput. Mater. Sci.*, 2012, **58**, 77–86.

22 J. B. A. Davis, S. L. Horswell and R. L. Johnston, *J. Phys. Chem. A*, 2013, **118**, 208–214.

23 I. Demiroglu, D. Stradi, F. Illas and S. T. Bromley, *J. Phys.: Condens. Matter*, 2011, **23**, 334215.

24 M. Aslan, Z. Öztürk and A. Sebetci, *J. Cluster Sci.*, 2014, **25**, 1187–1201.

25 J. B. A. Davis, R. L. Johnston, L. Rubinovich and M. Polak, *J. Chem. Phys.*, 2014, **141**, 224307.

26 C. Lueng, P. J. Metaxas and M. Kostylev, Conference on Optoelectronic and Microelectronic Materials and Devices (COMMAD), IEEE, 2014, pp. 27–29.

27 A. Prasad and P. J. Cascone, *U. S. Pat.* No. 8,623,272, U.S. Patent and Trademark Office, Washington, DC, 2014.

28 S. Ramaprabhu, B. A. R. O. Mridula, P. Nayak and T. T. Baby, *U. S. Pat.*, No. 9,149,833, U.S. Patent and Trademark Office, Washington, DC, 2015.

29 S. Akbayrak, M. Kaya, M. Volkan and S. Özkar, *Appl. Catal., B*, 2014, **147**, 387–393.

30 K. Mech, G. Boczkal, P. Pałka, P. Zabiński and R. Kowalik, *J. Solid State Electrochem.*, 2014, **18**, 3121–3127.

31 B. Li, X. Liu, M. Zhu, Z. Wang, A. Adeyeye and W. Choi, *J. Nanosci. Nanotechnol.*, 2015, **15**, 4332–4338.

32 H. Yildirim, A. Kara and T. S. Rahman, *J. Phys. Chem. C*, 2012, **116**, 281–291.

33 H. Arslan, *Int. J. Mod. Phys. C*, 2008, **19**, 1243–1255.

34 R. Ferrando, J. Jellinek and R. L. Johnston, *Chem. Rev.*, 2008, **108**, 845–910.

This journal is © the Owner Societies 2016

Phys. Chem. Chem. Phys., 2016, **18**, 6676–6682 | 6681

35 D. T. Tran and R. L. Johnston, *Proc. R. Soc. A*, 2011, **467**, 2004–2019.

36 S. Heiles and R. L. Johnston, *Int. J. Quantum Chem.*, 2013, **113**, 2091–2109.

37 F. Pittaway, L. O. Paz-Borbón, R. L. Johnston, H. Arslan, R. Ferrando, C. Mottet, G. Barcaro and A. Fortunelli, *J. Phys. Chem. C*, 2009, **113**, 9141–9152.

38 H. Cantera-López, J. M. Montejano-Carrizales, F. Aguilera-Granja and J. L. Morán-López, *Eur. Phys. J. D*, 2010, **57**, 61–69.

39 S. Bischoff, A. Weigt, K. Fujimoto and B. Lücke, *J. Mol. Catal. A: Chem.*, 1995, **95**, 259–268.

40 M. Heemeier, A. F. Carlsson, M. Naschitzki, M. Schmal, M. Bäumer and H.-J. Freund, *Angew. Chem., Int. Ed.*, 2002, **41**, 4073–4076.

41 F. B. Noronha, M. Schmal, C. Nicot, B. Moraweck and R. Frety, *J. Catal.*, 1997, **168**, 42–50.

42 P. Giannozzi, S. Baroni, N. Bonini, M. Calandra, R. Car, C. Cavazzoni, D. Ceresoli, G. L. Chiarotti, M. Cococcioni and I. Dabo, *J. Phys.: Condens. Matter*, 2009, **21**, 395502.

43 D. Deaven and K. Ho, *Phys. Rev. Lett.*, 1995, **75**, 288.

44 A. M. Rappe, K. M. Rabe, E. Kaxiras and J. Joannopoulos, *Phys. Rev. B: Condens. Matter Mater. Phys.*, 1990, **41**, 1227.

45 P. E. Blöchl, *Phys. Rev. B: Condens. Matter Mater. Phys.*, 1994, **50**, 17953.

46 J. P. Perdew, K. Burke and M. Ernzerhof, *Phys. Rev. Lett.*, 1996, **77**, 3865.

47 M. Methfessel and A. Paxton, *Phys. Rev. B: Condens. Matter Mater. Phys.*, 1989, **40**, 3616.

48 M. Valiev, E. J. Bylaska, N. Govind, K. Kowalski, T. P. Straatsma, H. J. Van Dam, D. Wang, J. Nieplocha, E. Apra and T. L. Windus, *Comput. Phys. Commun.*, 2010, **181**, 1477–1489.

49 P. J. Hay and W. R. Wadt, *J. Chem. Phys.*, 1985, **82**, 270–283.

50 W. R. Wadt and P. J. Hay, *J. Chem. Phys.*, 1985, **82**, 284–298.

51 A. Kant and B. Strauss, *J. Chem. Phys.*, 1964, **41**, 3806–3808.

52 L. M. Russon, S. A. Heidecke, M. K. Birke, J. Conceicao, M. D. Morse and P. Armentrout, *J. Chem. Phys.*, 1994, **100**, 4747–4755.

53 K. A. Gingerich, *Faraday Symp. Chem. Soc.*, 1980, **14**, 109–125.

54 S. Taylor, E. M. Spain and M. D. Morse, *J. Chem. Phys.*, 1990, **92**, 2698–2709.

55 K. Koyasu, M. Mitsui, A. Nakajima and K. Kaya, *Chem. Phys. Lett.*, 2002, **358**, 224–230.

56 B. Sahu, G. Maofa and L. Kleinman, *Phys. Rev. B: Condens. Matter Mater. Phys.*, 2003, **67**, 115420.

57 C. Jamorski, A. Martinez, M. Castro and D. R. Salahub, *Phys. Rev. B: Condens. Matter Mater. Phys.*, 1997, **55**, 10905.

58 M. Castro, C. Jamorski and D. R. Salahub, *Chem. Phys. Lett.*, 1997, **271**, 133–142.

59 A. Sebetci, *Chem. Phys.*, 2008, **354**, 196–201.

60 M. Pereiro, D. Baldomir, M. Iglesias, C. Rosales and M. Castro, *Int. J. Quantum Chem.*, 2001, **81**, 422–430.

61 S. Datta, M. Kabir, S. Ganguly, B. Sanyal, T. Saha-Dasgupta and A. Mookerjee, *Phys. Rev. B: Condens. Matter Mater. Phys.*, 2007, **76**, 014429.

62 R. Van Zee, Y. Hamrick, S. Li and W. Weltner, *Chem. Phys. Lett.*, 1992, **195**, 214–220.

63 Q. M. Ma, Z. Xie, J. Wang, Y. Liu and Y. C. Li, *Phys. Lett. A*, 2006, **358**, 289–296.

64 G. Qiu, M. Wang, G. Wang, X. Diao, D. Zhao, Z. Du and Y. Li, *THEOCHEM*, 2008, **861**, 131–136.

65 M. Moseler, H. Häkkinen, R. N. Barnett and U. Landman, *Phys. Rev. Lett.*, 2001, **86**, 2545–2548.

66 Q.-M. Ma, Z. Xie, J. Wang, Y. Liu and Y.-C. Li, *Phys. Lett. A*, 2006, **358**, 289–296.

67 S. Datta, M. Kabir, T. Saha-Dasgupta and A. Mookerjee, *Phys. Rev. B: Condens. Matter Mater. Phys.*, 2009, **80**, 085418.

68 J. Jalink, *Metal clusters: from geometric to electronic and magnetic properties*, Doctoral Thesis, Radboud University Nijmegen, Netherlands, 2014.

69 G. Zanti and D. Peeters, *Eur. J. Inorg. Chem.*, 2009, 3904–3911.

70 P. Begum, D. Bhattacharjee, B. K. Mishra and R. C. Deka, *Theor. Chem. Acc.*, 2014, **133**, 1–11.

71 J. Moc, D. G. Musaev and K. Morokuma, *J. Phys. Chem. A*, 2003, **107**, 4929–4939.

72 J. Rodríguez-López, F. Aguilera-Granja, K. Michaelian and A. Vega, *Phys. Rev. B: Condens. Matter Mater. Phys.*, 2003, **67**, 174413.

73 C. Kittel, *Introduction to solid state physics*, Wiley, 2005.

74 Q. L. Lu, L. Z. Zhu, L. Ma and G. H. Wang, *Phys. Lett. A*, 2006, **350**, 258–262.

75 H. Arslan, A. K. Garip and R. L. Johnston, *Phys. Chem. Chem. Phys.*, 2015, **42**, 28311–28321.

76 E. Janssens, T. Van Hoof, N. Veldeman, S. Neukermans, M. Hou and P. Lievens, *Int. J. Mass Spectrom.*, 2006, **252**, 38–46.

77 P. Nava, M. Sierka and R. Ahlrichs, *Phys. Chem. Chem. Phys.*, 2003, **5**, 3372–3381.

78 C. Luo, C. Zhou, J. Wu, T. Dhilip Kumar, N. Balakrishnan, R. C. Forrey and H. Cheng, *Int. J. Quantum Chem.*, 2007, **107**, 1632–1641.

79 M. B. Knickelbein, *J. Chem. Phys.*, 2006, **125**, 44308.

80 B. Kalita and R. C. Deka, *J. Chem. Phys.*, 2007, **127**, 244306.

81 S. Yin, R. Moro, X. Xu and W. A. de Heer, *Phys. Rev. Lett.*, 2007, **98**, 113401.

82 V. Bakken and O. Swang, *J. Chem. Phys.*, 2008, **128**, 084712.

83 A. Shayeghi, D. Götz, J. Davis, R. Schaefer and R. L. Johnston, *Phys. Chem. Chem. Phys.*, 2015, **17**, 2104–2112.

84 J. B. Davis, A. Shayeghi, S. L. Horswell and R. L. Johnston, *Nanoscale*, 2015, **7**, 14032–14038.

6682 | *Phys. Chem. Chem. Phys.*, 2016, **18**, 6676–6682

This journal is © the Owner Societies 2016